Expediting Corrosion Engineering for Sulfur-Doped, Self-Supporting Ni-Fe Layered Dihydroxide in Efficient Aqueous Oxygen Evolution

Yingjun Ma [1,2], **Jie Wang** [1,2,3,*], **Hangning Liu** [2], **Lin Wang** [2], **Changhui Sun** [2], **Liangyu Gong** [2], **Xiaogang Zhang** [1,*] **and Jiefang Zhu** [3,*]

[1] Jiangsu Key Laboratory of Electrochemical Energy Storage Technology, College of Material Science and Engineering, Nanjing University of Aeronautics and Astronautics, Nanjing 210016, China; myj3752@163.com

[2] Qingdao Engineering Research Center of Agricultural Recycling Economy Materials, College of Chemistry and Pharmaceutical Sciences, Qingdao Agricultural University, Qingdao 266109, China; 20200201033@stu.qau.edu.cn (H.L.); wlinlin990304@163.com (L.W.); sunchanghui123@stu.qau.edu.cn (C.S.); lygong@163.com (L.G.)

[3] Department of Chemistry, Ångström Laboratory, Uppsala University, 75121 Uppsala, Sweden

* Correspondence: wangjie@qau.edu.cn (J.W.); azhangxg@nuaa.edu.cn (X.Z.); jiefang.zhu@kemi.uu.se (J.Z.)
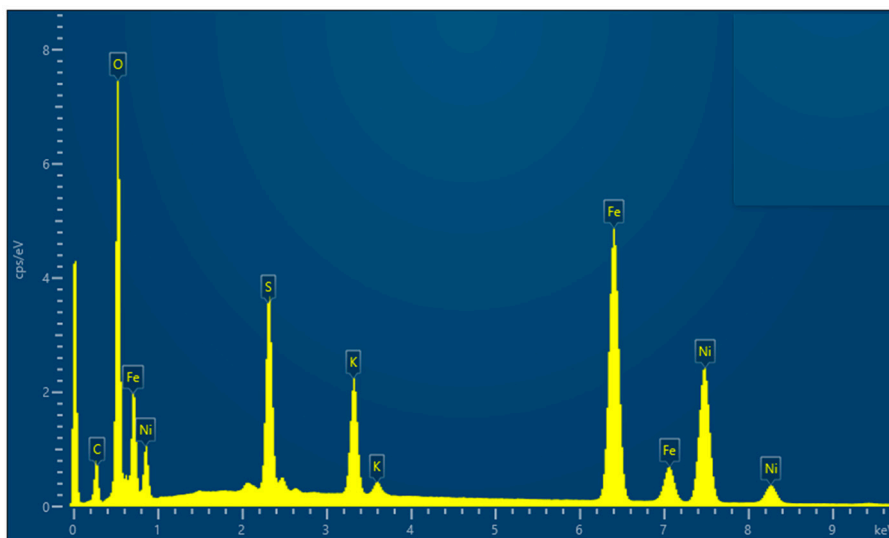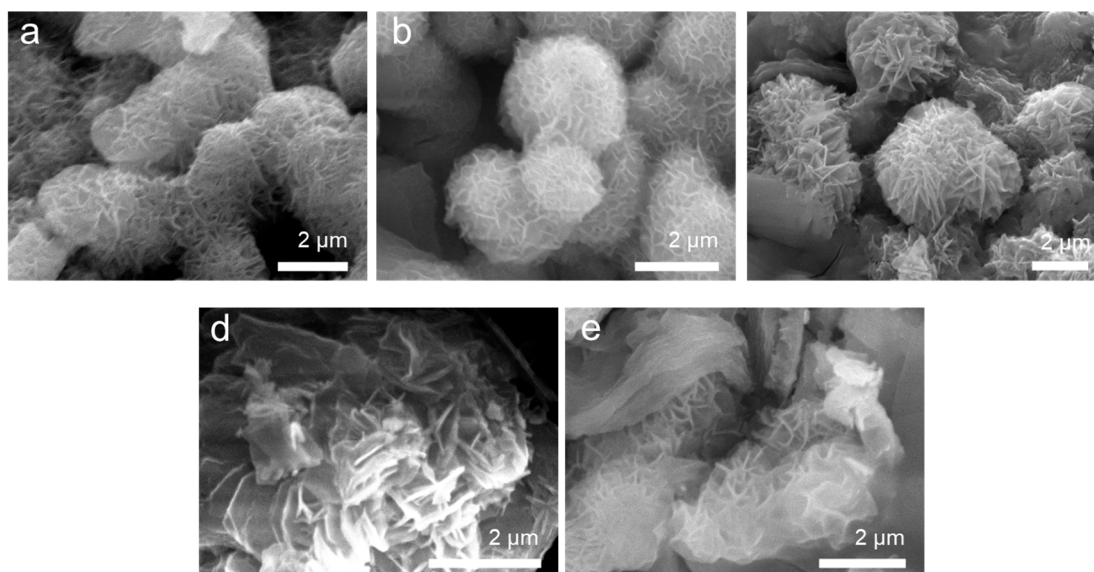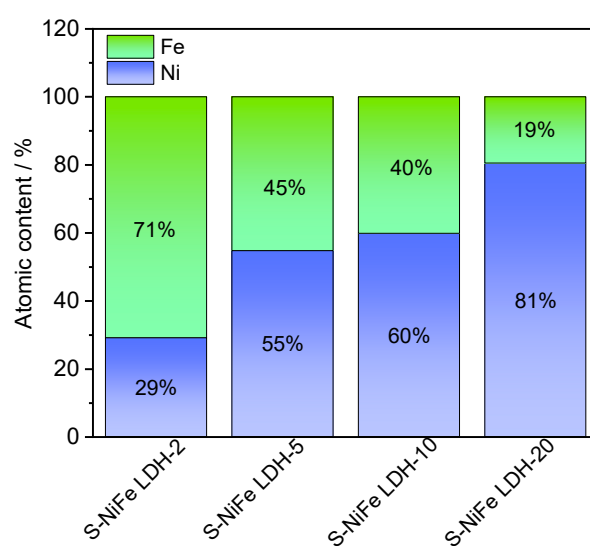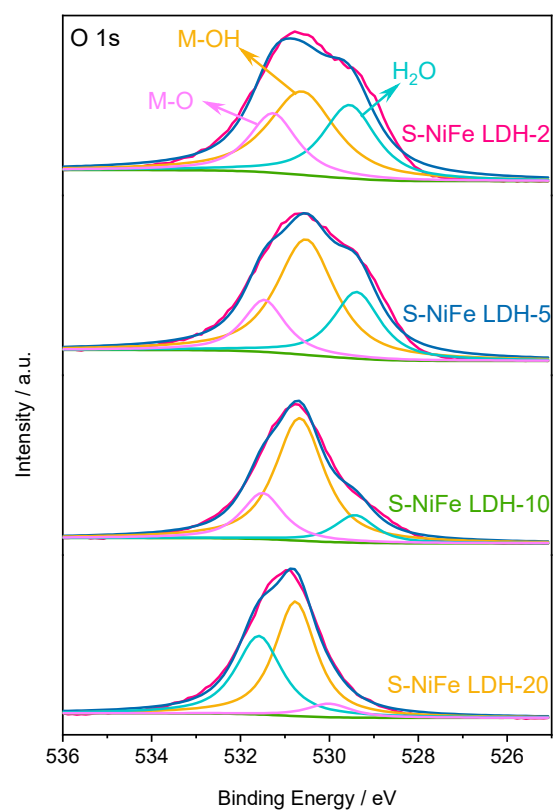
Figure S1 EDS spectrum of NiFe LDH characterized via SEM technique.
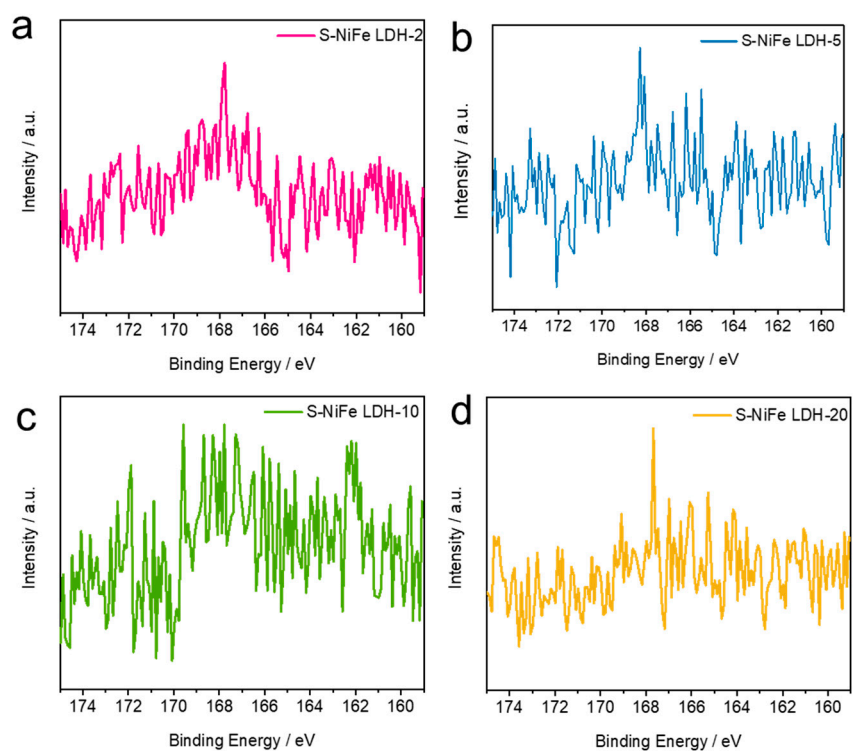
Figure S2 SEM images of S-NiFe LDH-2 h (a); S-NiFe LDH-4 h (b); S-NiFe LDH-6 h (c); S-NiFe LDH-8 h (d); and S-NiFe LDH-10 h (e).
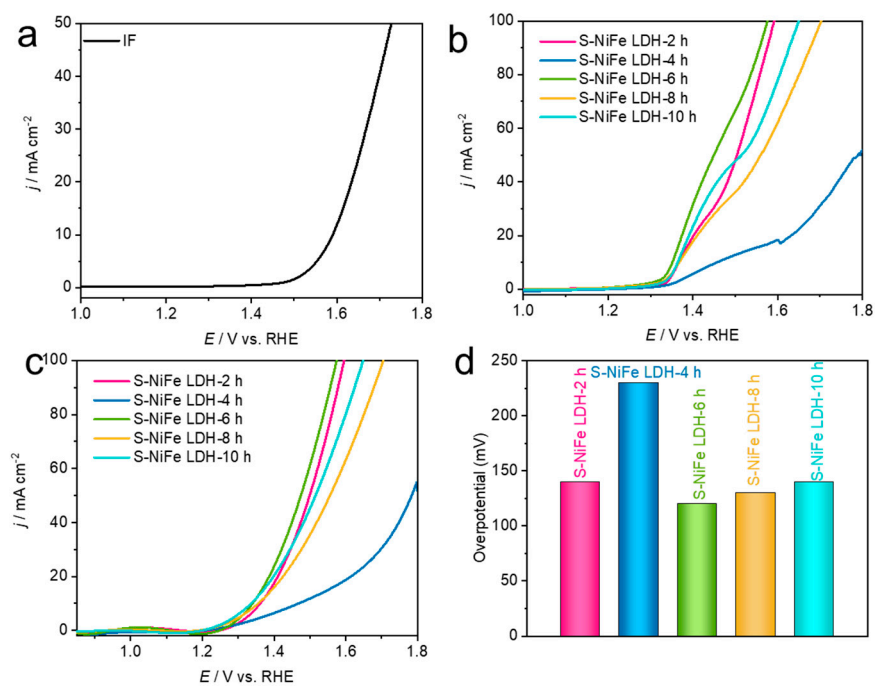

Figure S3 Atomic contents of Ni and Fe obtained from XPS survey spectra of Figure 4a.

Figure S4 High-resolution O 1s XPS spectra of S-NiFe LDH-2, S-NiFe LDH-5, S-NiFe LDH-10 and S-NiFe LDH-20.

Figure S5 High-resolution S 2p XPS spectra of S-NiFe LDH-2 (a), S-NiFe LDH-5 (b), S-NiFe LDH-10 (c), and S-NiFe LDH-20 (d).

Figure S6 (a) Polarization curves of pure IF;(b) Polarization curves of S-NiFe LDH-2h, S-NiFe LDH-4h, S-NiFe LDH-6h, S-NiFe LDH-8h, S-NiFe LDH-10h and fitted (c); (d) Corresponding overpotential histogram of the four catalysts at a current density of 10 mA cm^{-2}.
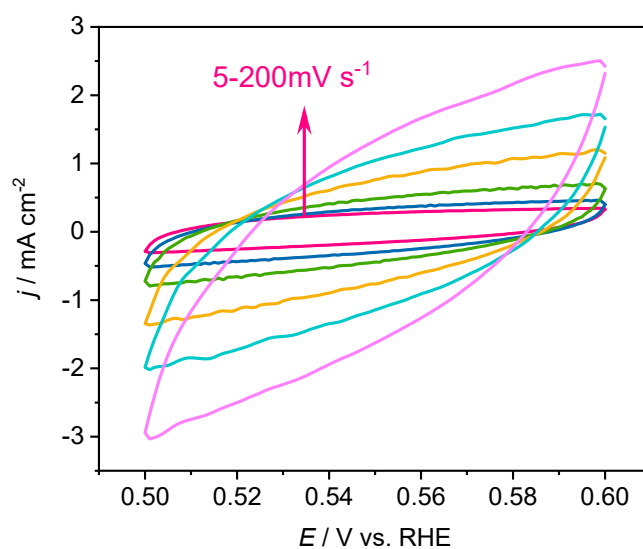
Figure S7 CV curves of pure S-NiFe LDH-2 at different scanning rates.
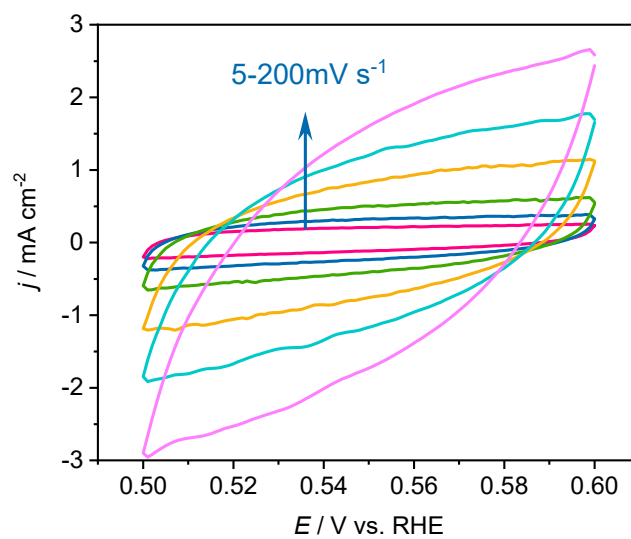
Figure S8 Cyclic voltammetry curves of pure S-NiFe LDH-5 at different scanning rates.
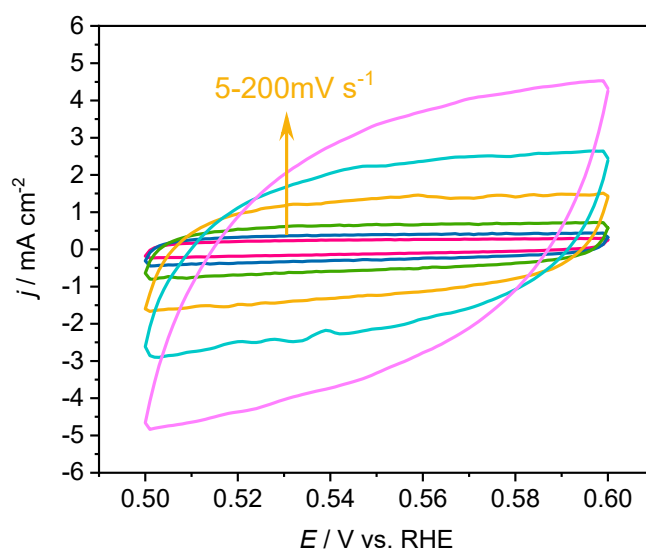
Figure S9 CV curves of S-NiFe LDH-10 at a potential window from 1.0 to 1.1 V under different scan rates.
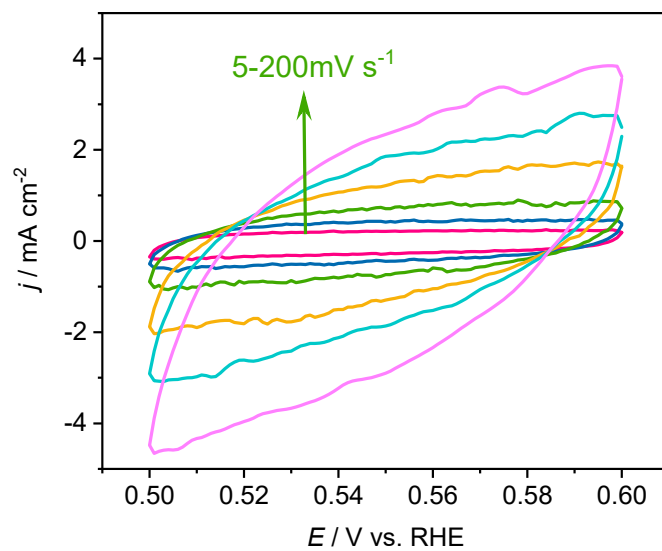
Figure S10 Cyclic voltammetry curves of pure S-NiFe LDH-20 at different scanning rates.

Figure S11 EIS spectrum of S-NiFe LDH catalysts obtained at different reaction times.

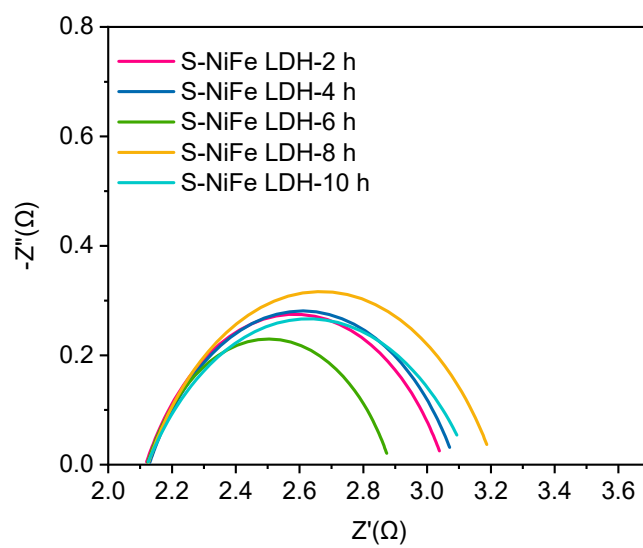**Table S1** Synthesis conditions of the S-NiFe-LDH catalysts.

Samples	Concentration of $Na_2S_2O_3$ (mM)	Concentration of $NiCl_2$ (mM)	Loading amount (mg cm^{-2})
S-NiFe LDH-2	0.03	2	26.9
S-NiFe LDH-5	0.03	5	20.4
S-NiFe LDH	0.03	10	29.4
S-NiFe LDH-20	0.03	20	17.8
S-NiFe LDH-2h	0.03	10	27.7
S-NiFe LDH-4h	0.03	10	26.5
S-NiFe LDH-8h	0.03	10	20.6
S-NiFe LDH-10h	0.03	10	12.4

Table S2 Elemental composition of S-NiFe LDH characterized by EDS.

Elements	at.%
Ni	10.5
Fe	14.4
S	5.6
O	69.5

Table S3 R_{ct} values of eight prepared catalysts derived from the EIS spectrum.

Catalysts	R_{ct}/Ω
S-NiFe LDH-2	0.91
S-NiFe LDH-5	0.78
S-NiFe LDH	0.75
S-NiFe LDH-20	0.79
S-NiFe LDH-2 h	0.92
S-NiFe LDH-4 h	0.94
S-NiFe LDH-8 h	1.06
S-NiFe LDH-10 h	0.97

Table S4 Comparative electrochemical OER performances of different electrocatalytic materials in alkaline medium.

Catalysts	Current density (mAcm^{-2})	Overpotential (mV)	Ref.
S-NiFe LDH	10	120	This work
	50	220	
Mn-RuO$_2$	10	270	1
Ru/RuO$_2$@N-rGO	10	255	2
(Co$_{0.5}$Ni$_{0.5}$)$_3$(PO$_4$)$_2$/Ni	10	273	3
NiFe LDH@ITO	10	240	4
NiFeCo-LDH/CF	10	249	5
NiS@SLS	10	297	6
Co$_{0.25}$Fe$_{0.75}$S$_2$	10	370	7
Ni$_3$S$_2$-NiFe LDHs/NF-2	50	230	8
FeOOH-a@NiFe LDHs	50	237	9
NiFe LDH/NiTe	50	228	10

1. Zhou, C.H.; Chen, X.; Liu, S.; Han, Y.; Meng, H.B.; Jiang, Q.Y.; Zhao, S.M.; Wei, F.; Sun, J.; Tian, T.; Zhang, R.F. Superdurable Bifunctional Oxygen Electrocatalyst for HighPerformance Zinc−Air Batteries. *J. Am. Chem. Soc.* **2022**, *144*, 2694-2704.
2. Gao, X.Y.; Chen, J.; Sun, X.Z.; Wu, B.F.; Li, B.; Ning, Z.C.; Li, J.; Wang, N. Ru/RuO$_2$ Nanoparticle Composites with N-Doped Reduced Graphene Oxide as Electrocatalysts for Hydrogen and Oxygen Evolution. *ACS Appl. Nano Mater.* **2020**, *3*, 12269-12277.
3. Li, J.W.; Xu, W.M.; Zhou, D.; Luo, J.X.; Zhang, D.W.; Xu, P.M.; Wei, L.C.; Yuan, D.S. Synthesis of 3D flower-like cobalt nickel phosphate grown on Ni foam as an excellent electrocatalyst for the oxygen evolution reaction. *J. Mater. Sci.* **2018**, *53*, 2077-2086.
4. Xu, J.C.; Li, Z.L.; Chen, D.; Yang, S.X.; Zheng, K.W.; Ruan, J.X.; Wu, Y.L.; Zhang, H.; Chen, J.; Xie, F.Y.; Jin, Y.S.; Wang, N.; Meng, H. Porous Indium Tin Oxide-Supported NiFe LDH as a Highly Active Electrocatalyst in the Oxygen Evolution Reaction and Flexible Zinc−Air Batteries. *ACS Appl. Mater. Interfaces* **2021**, *13*, 48774-48783.

5. Lin, Y.P.; Wang, H.; Peng, C.K.; Bu, L.M.; Chiang, C.L.; Tian, K.; Zhao, Y.; Zhao, J.Q.; Lin, Y.G.; Lee, J.M.; Gao, L.J. Co-Induced Electronic Optimization of Hierarchical NiFe LDH for Oxygen Evolution. *Small* **2021**, *16*, 2002426.

6. Chen, J.S.; Ren, J.; Shalom, M.; Fellinger, T.; Antonietti, M. Stainless Steel Mesh-Supported NiS Nanosheet Array as Highly Efficient Catalyst for Oxygen Evolution Reaction. *ACS Appl. Mater. Interfaces* **2016**, *8*, 5509-16.

7. Gao, L.; Guo, C.; Liu, X.; Ma, X.; Zhao, M.; Kuang, X.; Yang, H.; Zhu, X.; Sun, X.; Wei, Q. Co-Doped FeS_2 with a porous structure for efficient electrocatalytic overall water splitting. *New J. Chem.* **2020**, *44*, 1711-1718.

8. Wu, S.W.; Liu, S.Q.; Tan, X.H.; Zhang, W.Y.; Cadien, K.; Li, Z. Ni_3S_2-embedded NiFe LDH porous nanosheets with abundant heterointerfaces for high-current water electrolysis. *Chem. Eng. J.* **2022**, *442*, 136105.

9. Zhao, M.H.; Wang, Y.N.; Mi, W.L.; Wu, J.T.; Zou, J.J.; Zhu, X.D.; Gao, J.; Zhang, Y.C. Surface-modified amorphous FeOOH on NiFe LDHs for high efficiency electrocatalytic oxygen evolution. *Electrochim. Acta* **2023**, *458*, 142513.

10. Hu, L.Y.; Zeng, X.; Wei, X.Q.; Wang, H.J.; Wu, Y.; Gu, W.L.; Shi, L.; Zhu, C.Z. Interface engineering for enhancing electrocatalytic oxygen evolution of NiFe LDH/NiTe heterostructures. *Appl. Catal. B-Environ.* **2020**, *273*, 119014.